Scientific
Research
Publishing

A Density Functional Theory (DFT) Investigation on the Structure and Spectroscopic Behavior of 2-Aminoterephthalic Acid and Its Sodium Salts

Mohammad A. Matin[1], Samiran Bhattacharjee[1*], Md. Aftab Ali Shaikh[2], Tapas Debnath[3], Mohammed Abdul Aziz[3]

[1]Centre for Advanced Research in Sciences (CARS), University of Dhaka, Dhaka, Bangladesh
[2]Department of Chemistry, University of Dhaka, Dhaka, Bangladesh
[3]Department of Theoretical and Computational Chemistry, University of Dhaka, Dhaka, Bangladesh
Email: *s.bhattacharjee@du.ac.bd

Abstract

As a substitute for lithium ion batteries, Na chemistry for ion battery systems is promising materials for energy storage applications for the next generation. Herein, the structures, IR and UV-visible spectra of 2-aminoterephthalic acid (H_2ATA), disodium 2-aminoterephthalate (Na_2ATA), trisodium 2-aminoterephthalate (Na_3ATA) and tetrasodium 2-aminoterephthalate (Na_4ATA) have been studied using density functional theory (DFT/B3LYP/6-311++G(d,p)). The theoretical geometric parameters and FTIR results showed very good agreement with the experimental results. Different conformers of Na_2ATA, Na_3ATA and Na_4ATA showed that the binding energy per sodium in Na_2ATA, Na_3ATA and Na_4ATA is −694.94, −543.44 and −407.46 kJ/mol, respectively. The Na_3ATA and Na_4ATA salts are higher in energy (151.46 and 287.48 kJ/mol, respectively) than Na_2ATA, indicating the higher stability of the Na_2ATA complex. The calculated binding energy, enthalpy and Gibbs free energy of Na_2ATA, Na_3ATA and Na_4ATA revealed that the compounds are thermodynamically stable. Natural bond orbital (NBO) analysis of Na_2ATA, Na_3ATA and Na_4ATA indicated that the major interaction occurs between the lone pair electrons of the oxygen atom and anti-bonding orbitals of carbon atoms of the two carboxylate ions. UV-visible spectrum of the free H_2ATA and its sodium salts Na_2ATA, Na_3ATA and Na_4ATA were performed using the time-dependent density functional theory (TD-DFT) method at the level of B3LYP/6-311++G(d,p). The frontier molecular orbital energetic parameters and global reactivity descriptors revealed that the Na_4ATA and

Na$_3$ATA complexes exhibited a higher band gap (ΔE_{gap}) and electronegativity (χeV) than Na$_2$ATA.

Keywords

2-Aminoterephthalic Acid, Sodium 2-Aminoterephthalate, Trisodium
2-Aminoterephthalate, Tetrasodium 2-Aminoterephthalate, Density
Functional Theory

1. Introduction

Much attention has recently been paid to the establishment of environmentally friendly more acceptable routes, including removal of toxic reagents, minimization of by-product formation, low cost, green and easy procedure. Batteries play an important role as a power source in our everyday life such as mobile phones, microgrids, satellites, etc. Among the various metal ion batteries, lithium-ion batteries are comparatively mature technology having high energy density, power density and good long cycle life [1], but the high cost and low availability of certain materials are its main disadvantages [2]. Due to low cost and high natural abundance of sodium, the sodium ion batteries (SIBs) have gained much attention in recent years as an economically interesting alternative to lithium ion batteries for the future exploration [2] [3]. Recently, various cathode materials for sodium ion batteries have been studied, viz., olivine-type sodium metal phosphates, prussian blue, Na$_3$V$_2$(PO$_4$)$_3$/carbon, Cu-doped P2-Na$_{0.5}$Ni$_{0.33}$Mn$_{0.67}$O$_2$ encapsulated with MgO and titanium substituted P2-Type Na$_{0.67}$Fe$_{0.5}$Mn$_{0.5}$O$_2$ [4]-[9]. For anode materials in SIBs, carbon-based materials (such as graphene, hard carbon, carbon nanosheet and hollow carbon nanospheres), Na$^+$ intercalation pseudocapacitance in TiO$_2$/graphene nanocomposites, amorphous phosphorus/carbon, carbon coated K$_{0.8}$Ti$_{1.73}$Li$_{0.27}$O$_4$ and carbon-coated NaTi$_2$(PO$_4$)$_3$ have been investigated [10]-[17]. Nanostructured and nanocomposites of organic conducting polymers have been studied in energy storage areas due to their numerous active sites which can generate green batteries with large capacity, high energy and long cycle life [18] [19] [20] [21]. A group of researchers reported the electrochemical performance of organic tetralithium salts of 2, 5-dihydroxyterephthalic acid having different morphologies viz., nanosheets, nanoparticles and bulk, as both positive and negative electrode of rechargeable lithium-ion batteries [22]. They observed that nanosheets morphologies exhibited the best electrochemical performance with discharge capacities of 223 and 145 mAh·g^{-1} at 0.1 and 5 C rates, respectively. Other organic electrode materials, such as, sodium salt of terephthalate and its various derivatives have been used as anode materials in sodium-ion batteries, which were prepared using simple acid-base chemistry [23]. These materials showed outstanding electrochemical activity [24]. In addition, tin, antimony and phosphorus easily formed alloy with

sodium, which exhibited excellent electrochemical performance as an anode material for Na-ion batteries [24] [25] [26] [27]. Very recently, Li *et al.* described the sodium-ion storage on CuS nanosheets anchored into reduced graphene oxide as anode for SIBs [28]. These materials showed high specific capacity, high initial Coulombic efficiency, superior rate performance and excellent long-term cycle stability, suggesting that Na chemistry for ion battery systems will be feasible for energy storage applications for the next generation. As derivatives of terephthalic acid, the 2-aminoterephthalic acid (H_2ATA) have been used for organic building block for assembly of metal-organic framework compounds (for example, isoreticular metal-organic framework-3, IRMOF-3), in which $-NH_2$ groups of organic linker do not involve in the construction of framework structure [29] [30]. Most importantly, this uncoordinated amine group can serve as an active catalyst site for a variety of organic reactions [31] [32] [33] [34] [35] and also show as a selective adsorbent for harmful gases [36]. Karabacak *et al.* described the experimental and theoretical vibrational and electronic analysis of 2-aminoterephthalic acid [37]. Recently, Renault *et al.* reported the application of dilithium 2-aminoterephthalate as organic Li-battery anode material [38]. The resulting electrodes showed stable capacities (ca. 180 mAh·g^{-1}) and excellent rate capabilities with battery performance at 500 mA·g^{-1}. The above results encouraged us to carry out the detailed theoretical calculations of 2-aminoterephthalate (H_2ATA) and its sodium salts, aim to find out a sustainable, green and low-cost route towards the construction of sodium ion batteries.

In this study, we report the theoretical calculations of H_2ATA, disodium 2-aminoterephthalate (Na_2ATA) and its sodium inserted complexes (trisodium 2-aminoterephthalate, Na_3ATA and tetrasodium 2-aminoterephthalate, Na_4ATA) using Density Functional Theory (DFT) with the hybrid B3LYP method to calculate a wide variety of molecular properties such as optimized structure, binding energy (ΔE) per sodium and spectroscopic properties. NBO (natural bond orbital) analysis and global reactivity descriptors of 2-aminoterephthalic acid, disodium 2-aminoterephthalate and its inserted sodium complexes (Na_3ATA and Na_4ATA) were also performed to evaluate the strength of donor-acceptor interaction energy and chemical reactivity of this compound. Electronic properties and UV-Visible spectra were also calculated. To our knowledge, there has been no systematic theoretical study of 2-aminoterephthalic acid and its sodium salts using Density Functional Theory (DFT).

2. Computational Details

The geometries of the model complexes were optimized at the hybrid B3LYP [39] method based on Becke's three-parameter functional of density functional theory (DFT) calculations using 6-311++G(d,p) basis set. Several structural configurations were considered for comparison of their stability. Geometry optimization was taken to be converged if the maximal atomic force was smaller than 0.00045 hartree/Bohr. Geometries of individual species ligand, metal and met-

al-complexes were optimized. No geometric constraint was imposed in all the calculations. After optimizing the geometry of each coordination complex, the metal–ligand binding energy ΔE was calculated as [40].

$$\Delta E = -\frac{\left(E_{\text{complex}} - E_{\text{metal}} - E_{\text{ligand}}\right)}{n}$$

where, E_{complex}, E_{metal} and E_{ligand} are the energies of the sodium terephthalate complex, the metal ion and terephthalate ligand, respectively. Therefore, states to the binding energy of the complex per sodium.
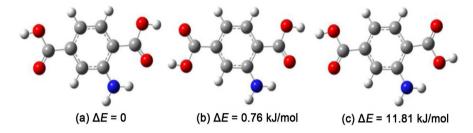
The vibrational frequency analyses were performed for all optimized structures (no imaginary frequencies), and indicating that the structures are stable minima on the potential energy surface. It is known that DFT potentials systematically overestimate the vibrational wavenumbers. These discrepancies are corrected either by computing anharmonic corrections explicitly or by introducing a scaled field or by directly scaling the calculated wavenumbers with a proper factor. The raw vibrational frequencies were scaled by a factor of 0.9580, which produced good agreement with the experiment for a wide range of systems. All calculations were performed using the Gaussian 16 program package [41]. Gauss View 6.0.16 was used for the visualization of the optimized structures and simulated vibrational spectra.

Electronically excited state calculations were performed to examine the UV-visible spectra of the H_2ATA molecule and its sodium salts. The vertical excitation energies were obtained using the time-dependent density functional theory (TD-DFT) at the level of B3LYP with the 6-311++G(d,p) basis set, after the ground-state optimization. Molecular orbital analysis was also done to calculate the HOMO-LUMO energy gap. Natural bond orbital analysis was performed to provide the appropriate scheme for the metal-ligand interactions. The global reactivity descriptors were also analyzed to describe the molecular reactivity.

3. Results and Discussions

3.1. Geometry of H₂ATA

The three different optimized conformers of H_2ATA together with their energy with respect to the most stable structure are illustrated in **Figures 1(a)-(c)**. **Figure 1(a)** is the most stable structure with minimum energy conformer where the C=O groups are on the same side. The second (**Figure 1(b)**) and third (**Figure 1(c)**) conformers are more than 0.76 and 11.81 kJ/mol, respectively, higher in energy than conformer 1a. The optimized geometrical parameters in both gas phase and different solvents are listed in **Table 1**. The bond lengths of both C-COOH (1) and C-COOH (2) in gas phase are slightly shorter (ca. 0.02Å) than experimental results (**Table 1**) [37]. Due to solvent effects, this bond length decreases almost by 0.018 Å than experimental. The C-NH₂ bond lengths both in gas phase and different solvents are calculated about 0.005 Å shorter than experimental result. There are no significant effects of solvents. Due to Coulombic interaction between O and H of COOH bond, C-O bond was calculated larger

than C=O bond. The C=O bond is 0.005Å larger than experimental results and no such significant difference was found in other solvents. The calculated bond angles of two carboxylates are found to be 1.83° and 1.68° shorter than experimental results [37]. It is also noticed that the calculated bond angles in different solvents varies by 1.50° and 1.44° respectively. These calculated values are good agreements with the experimental results [37] except the NH_2 bond angles which are predicted shorter by 1.78° in gas phase and almost 2.90° in different solvents.

Figure 1. Theoretical optimized minimum energy conformer of the H_2ATA. Grey, white, blue and red circles represent carbon, hydrogen, nitrogen and oxygen, respectively.
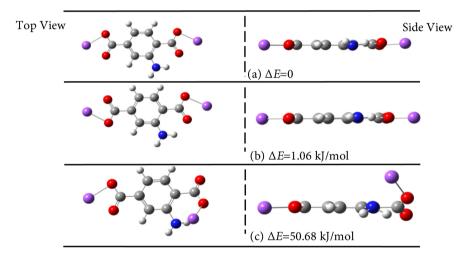
Table 1. Comparison of the theoretical (optimized) and experimental geometric parameters of H_2ATA in gas phase and different solvents.

Medium[a]	Molecular Geometry[b]					
	$d_{(C-O)}$ (Å)	$d_{(C=O)}$ (Å)	$d_{(C-N)}$ (Å)	$d_{(Cg-C)}$ (Å)	$\theta_{(COO)}$ (deg.)	$\theta_{(NH_2)}$ (deg.)
Gas	1.356 1.355	1.208 1.221	1.361	1.469 1.492	120.47 122.12	120.22
DMF	1.351 1.348	1.213 1.223	1.361	1.471 1.493	120.80 122.36	119.10
DMSO	1.351 1.348	1.213 1.223	1.360	1.471 1.493	120.80 122.36	119.10
EtOH	1.352 1.349	1.212 1.223	1.360	1.471 1.492	120.75 122.31	119.38
EtSH	1.352 1.349	1.212 1.223	1.360	1.471 1.492	120.75 122.31	119.38
Pyridine	1.351 1.348	1.213 1.223	1.360	1.471 1.493	120.78 122.34	119.20
FA	1.351 1.347	1.213 1.223	1.361	1.471 1.493	120.81 122.36	119.07
NBA	1.353 1.349	1.212 1.222	1.360	1.471 1.492	120.72 122.29	119.43
ACN	1.351 1.347	1.213 1.223	1.361	1.471 1.493	120.80 122.36	119.11
Exper.	1.330 1.333	1.195 1.216	1.365	1.489 1.512	122.3 123.8	122.0

[a] DMF = dimethylformamide, DMSO = dimethyl sulfoxide, EtOH = ethanol, EtSH = ethanethiol, FA = formamide, NBA = n-butylamine, ACN = acetonitrile. [b] d = bond length, d(Cg-C) = d(C_{ring}-C), θ = bond angle.
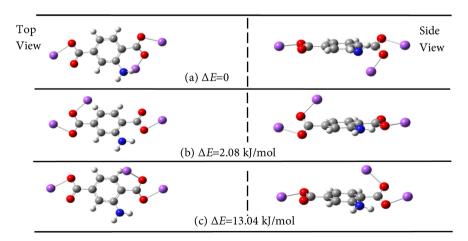
3.2. Geometries of Sodium Salts

The three different optimized structures of disodium 2-aminoterephthalate (Na_2 ATA), sodium inserted complexes trisodium (Na_3ATA) and tetrasodium (Na_4 ATA) 2-aminoterephthalate were shown in **Figures 2-4** and the results were summarized in **Table 2**. A significant change of bond lengths of C-N and C_{ring}-C were observed in disodium, trisodium and tetrasodium salts of H_2ATA. The C-N bond lengths of tetrasodium salt were 0.055 Å larger than disodium salt. A significant change of bond angle of NH_2 was observed in disodium and its sodium inserted complexes and about 8.18° larger in disodium complex compare to trisodium and tetrasodium complex.
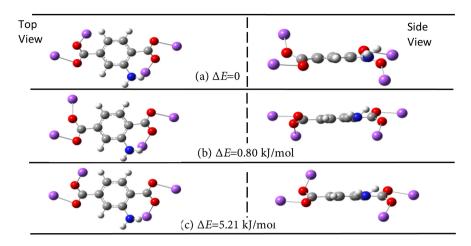
Different conformers of the $C_8H_5Na_xNO_4$ (x = 2, 3 or 4) were investigated by DFT calculations (**Figures 2-4**). In the case of $C_8H_5Na_2NO_4$, there is a negligible

Figure 2. Structures of disodium 2-aminoterephthalate (Na_2ATA). The three different conformations of Na_2ATA together with their energy with respect to the most stable structure. Grey, white, blue, red and purple circles represent carbon, hydrogen, nitrogen, oxygen and sodium atoms, respectively.

Figure 3. Structures of trisodium 2-aminoterephthalate (Na_3ATA). The three different conformations of Na_3ATA together with their energy with respect to the most stable structure.

Figure 4. Structures of tetrasodium 2-aminoterephthalate (Na$_4$ATA). The three different conformations of Na$_4$ATA together with their energy with respect to the most stable structure.

Table 2. Geometrical parameters of Na$_2$ATA, Na$_3$ATA and Na$_4$ATA (optimized lowest energy structure).

Complex	d_{C-O},s (Å)	d'_{C-N}s (Å)	$d'_{C_{ring}-C}$s (Å)	θ'_{COO}s (deg.)	θ_{NH_2} (deg.)
Na$_2$ATA	1.276	1.379	1.502	122.32	118.30
Na$_3$ATA	1.268	1.438	1.509	123.17	108.32
Na$_4$ATA	1.290	1.426	1.511	122.90	108.73

energy difference for the rotation of the carboxylate group in the meta position as compared to the amino group, but a relative increase in energy of 1.06 kJ/mol and 50.68 kJ/mol if the sodium is placed between the ortho-carboxylate and the amino group (**Figure 2(b)** and **Figure 2(c)**). The sodium ion naturally found in the unreduced carboxylate group, whereas retaining the energetically favorable location for one sodium atom near to the amino group.

According to **Table 3**, the binding energy, enthalpy and Gibbs free energy of Na$_2$ATA complex exhibit value on −694.94, −543.44 and −407.46 kJ/mol respectively and this suggests the thermodynamically most stability of the complex. The binding energies of Na$_3$ATA and Na$_4$ATA in the range of −543.44 to −407.46 kJ/mol, also suggest the thermodynamical stability. The per sodium energy difference of Na$_2$ATA is smaller (151.46 and 287.48 kJ/mol) compare to Na$_3$ATA and Na$_4$ATA, indicating the higher stability of the Na$_2$ATA complex. The binding energies, enthalpies and Gibbs free energy of disodium inserted complexes (Na$_3$ATA and Na$_4$ATA) are also tabulated in **Table 3**.

3.3. FTIR Spectra

The calculated infrared (IR) absorption frequencies of the compound and its sodium complexes in gasphase are listed in **Table 4** and the spectra are shown in **Figure 5**. The calculated wavenumbers are scaled by a factor of 0.9580. The strong bands at 3615 and 3611 cm^{-1} of free H$_2$ATA assigned to O-H stretching
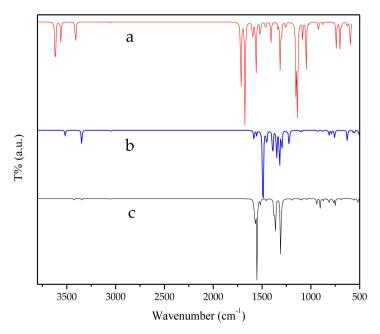
Table 3. Binding energy (ΔE), enthalpy (ΔH) and Gibbs free energy (ΔG) of Na$_2$ATA, Na$_3$ATA and Na$_4$ATA (optimized lowest energy structure).

Complex	ΔE (kJ/mol)	ΔH (kJ/mol)	ΔG (kJ/mol)
Na$_2$ATA	−694.94	−690.96	−657.90
Na$_3$ATA	−543.44	−539.73	−507.15
Na$_4$ATA	−407.46	−404.35	−372.96

Table 4. Characteristic IR bands (cm^{-1}) for H$_2$ATA, Na$_2$ATA, Na$_3$ATa and Na$_4$ATA[a].

Complex	ν(OH)	ν_{asy}(NH$_2$)	ν_{sy}(NH$_2$)	νC=O	ν_{asy}(C-O)	ν_{sy}(C-O)	ν(C=C)	ν(C-N)
H$_2$ATA	3615 3611	3555	3405	1711 1670	-	-	1493	1250
Na$_2$ATA	-	3562	3369	-	1491	1394	1584	1228
Na$_3$ATA		3534	3386		1574	1361	1591	1196
					1522	1342		
Na$_4$ATA	-	3529	3392	-	1566 1536	1367 1336	1587	1225

[a] ν = stretching vibration, ν_{asy} = asymmetric and ν_{sy} = symmetric.

Figure 5. Theoretical IR spectra of (a) free H$_2$ATA, (b) Na$_2$ATA and (c) Na$_4$ATA.

vibrations of carboxylic groups, were disappeared on metal carboxylate formation [42]. The strong bands at 1711 and 1670 cm^{-1} of free H$_2$ATA in FT-IR due to C=O stretching vibration are shifted to 1491 and 1394 cm^{-1} in the disodium 2-aminoterephthalate complex, Na$_2$ATA, correspond to asymmetric ν_{asy}(C-O) and symmetric ν_{sy}(C-O) vibrations, respectively [43]. On the other hand, both trisodium

2-aminoterephthalate (Na$_3$ATA) and the tetrasodium 2-aminoterephthalate, Na$_4$ATA, exhibited four bands at ca.1574 and ca.1522 cm^{-1}, and at ca.1361 and ca.1342 cm^{-1}, due to asymmetric ν_{asy}(C-O) and symmetric ν_{sy}(C-O) vibrations, respectively (Table 4). The FTIR spectra of H$_2$ATA and its sodium salts exhibited two bands at ca. 3550 and ca. 3390 cm^{-1} due to the amino group [44]. In addition, all compounds showed band at ca. 1230 cm^{-1} which may be assigned to the C-N stretching vibrations [45].

3.4. Natural Bond Orbital (NBO) Analysis

The NBO analysis was known to be effective tools for chemical elucidation of hyperconjugative interaction and electron density transfer from the filled lone pair electron [46]. Density Functional Theory with the hybrid B3LYP method was used for NBO calculation to examine the various second-order interactions between the filled orbitals of one subsystem andunoccupied orbital of another subsystem. NBO analysis of disodium, trisodium and tetrasodium 2-aminoterephthalate was carried out to evaluate the strength of donor-acceptor interaction energy, E(2) of these complexes and the results are summarized (disodium and tetrasodium only) in Table 5. The results showed the most effective interaction between the anti-bonding electrons of carbon (C$_4$-C$_5$) and carbon (C$_1$-C$_6$) of the π-conjugated system of the benzene ring. The results showed that the major interaction energies of this compound appeared from the interaction between the lone pair electrons of the O atom and antibonding orbitals of carbon atoms of the two carboxylate ions as well as sodium ions. There is also a significant

Table 5. Second order perturbation theory analysis of Fock matrix in NBO for the Na$_2$ATA and Na$_4$ATA in gas phase[a].

Complex	Na$_2$ATA			Na$_4$ATA			
Donor(i)-Acceptor(j) Interaction	E^2 (kJ/mol)	E_j-E_i (a.u.)	F_{ij} (a.u.)	Donor(i)-Acceptor(j) Interaction	E^2 (kJ/mol)	E_j-E_i (a.u.)	F_{ij} (a.u.)
$LP_{O10} \rightarrow LP^*_{C4-C5}$	65.65	0.72	0.096	$LP_{O10} \rightarrow BD^*_{C4-O11}$	83.55	0.75	0.111
$LP_{O10} \rightarrow LP^*_{C9}$	722.91	0.15	0.158	$LP_{O11} \rightarrow BD^*_{C9-O10}$	304.51	0.30	0.132
$LP_{O11} \rightarrow LP^*_{C9}$	617.35	0.15	0.152	$LP_{O13} \rightarrow BD^*_{C12-O14}$	283.55	0.31	0.130
$LP_{O13} \rightarrow LP^*_{C12}$	720.36	0.15	0.158	$LP_{O14} \rightarrow BD^*_{C12-O13}$	84.35	0.75	0.111
$LP_{O14} \rightarrow LP^*_{C12}$	710.61	0.15	0.158	$LP_{N16} \rightarrow BD^*_{C4-O5}$	69.16	0.38	0.077
$LP^*_{O10} \rightarrow LP^*_{Na12}$	16.07	0.76	0.006	$BD^*_{C4-C5} \rightarrow BD^*_{C1-C6}$	1270.14	0.01	0.083
$LP^*_{O11} \rightarrow LP^*_{Na12}$	16.23	0.79	0.050	$LP_{O13} \rightarrow LP^*_{C12}$	648.02	0.16	0.158
$LP^*_{O13} \rightarrow LP^*_{Na20}$	15.10	0.76	0.047	$LP_{O14} \rightarrow LP^*_{C12}$	656.80	0.16	0.158
$LP^*_{O14} \rightarrow LP^*_{Na20}$	15.10	0.76	0.047	$LP^*_{O10} \rightarrow LP^*_{Na19}$	13.68	0.82	0.046
				$LP_{O11} \rightarrow LP^*_{Na21}$	19.33	0.84	0.056
				$LP^*_{O13} \rightarrow LP^*_{Na20}$	14.94	0.81	0.048
				$LP^*_{O14} \rightarrow LP^*_{Na22}$	13.56	0.83	0.046

[a] LP = lone pair, LP* = antibonding lone pair, BD = bonding pair, BD* = antibonding.

interaction noticed with the lone pair electrons of nitrogen (amino group) to the anti-bonding of C_4-O_5.

3.5. Electronic Properties and UV-Visible Spectrum of H_2ATA, Na_2ATA and Sodium Inserted Complexes

The time-dependent DFT (TD-DFT) on electronic absorption spectrum of H_2ATA, Na_2ATA, Na_3ATA and Na_4ATA in gas phase were calculated using B3LYP/6-311++G(d,p) method. The major possible transitions, calculated frontier orbital energies, oscillator strengths (f), excitation energies (eV) and molecular orbital (MO) major contributions listed in Table 6 and Table 7 respectively. The energy gap between the orbitals demonstrated the molecular chemical stability which is critical parameters in determining the molecular electrical

Table 6. Calculated wavelengths (λ), oscillator strengths (f) and excitation energies (E) of H_2ATA, Na_2ATA, Na_3ATA and Na_4ATA at gas phase using TD-DFT/B3LYP/6-311++G(d,p) level of theory.

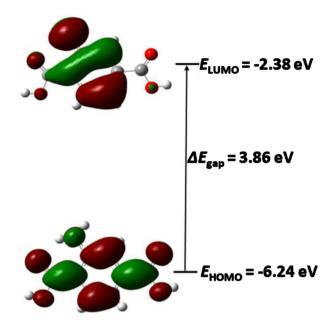| Complex	λ(nm)	E(eV)	f(Oscillator Strengths)	MO Contributions	Assignments
H_2ATA	225	5.52	0.3977	H → L+1(56%), H−1 → L(16%)	LLCT(π→π*)
	255	4.87	0.1297	H−1 → L(73%), H → L+1(25%)	LLCT(π→π*)
	260	4.76	0.0000	H−3 → L(90%), H−2 → L(4%)	LLCT(π→π*)
	270	4.59	0.0000	H−2 → L(91%), H−3 → L(4%)	LLCT(π→π*)
	365	3.39	0.0869	H → L(98%), H−1 → L+1(2%)	LLCT(n→π*)
Na_2ATA	260	4.76	0.1396	H−3 → L+2(46%), H−3 → L+1(16%)	LLCT(π→π^*)
	267	4.64	0.2047	H−3 → L+1(55%), H−6 → L+1(32%)	LLCT(π→π^*)
	272	4.55	0.0030	H → L+5(55%), H → L+6(40%)	LLCT(π→π^*)
	278	4.46	0.0026	H → L+3(70%), H → L+4(24%)	LLCT(π→π^*)
	285	4.35	0.0029	H → L+3(21%), H → L+4(50%)	LLCT(π→π^*)
	340	3.65	0.0989	H → L+2(96)	LLCT(n→π*)
Na_3ATA	235	5.28	0.0716	H−5 → L+1(70%)	LLCT(π→π*)
	251	4.93	0.0091	H → L+3(73%)	LLCT(π→π*)
	255	4.87	0.2060	H−5 → L+1(10%), H−3 → L+1(41%)	LLCT(π→π*)
	265	4.68	0.0252	H−2 → L+1(71%), H → L+3(18%)	LLCT(π→π*)
	288	4.31	0.0416	H−1 → L+1(88%)	LLCT(π→π*)
	307	4.03	0.0066	H−1 → L(89%)	LLCT(π→π*)
Na_4ATA	185	6.71	0.1024	H−4 → L+1(20%), H−1 → L+5(10%)	LLCT(π→π*)
	193	6.43	0.2045	H−1 → L+5(52%)	LLCT(π→π*)
	199	6.22	0.4060	H−1 → L+1(13%), H → L+5(37%)	LLCT(π→π*)
	219	5.66	0.0829	H−3 → L(10%), H−3 → L+1(33%)	LLCT(π→π*)
	228	5.43	0.0824	H → L(51%), H−3 → L+1(10%)	LLCT(π→π*)
	245	5.07	0.1268	H−1 → L(17%), H−1 → L+1(47%)	LLCT(π→π*)
	267	4.65	0.0523	H → L(17%), H → L+1(64%)	LLCT(π→π*)

Table 7. Frontier molecular orbital energetic parameters of free H$_2$ATA, Na$_2$ATA, Na$_3$ATA and Na$_4$ATA at gaseous state[a].

Complex	E_{HOMO}(eV)	E_{LUMO}(eV)	ΔE_{gap}(eV)	I(eV)	A(eV)
H$_2$ATA	−6.24	−2.38	3.86	6.24	2.38
Na$_2$ATA	−4.79	−1.47	3.32	4.79	1.47
Na$_3$ATA	−8.90	−4.35	4.55	8.90	4.35
Na$_4$ATA	−12.02	−7.03	4.99	12.02	7.03

[a] ΔE_{gap} = Energy gap, I = ionization potential, A = electron affinity.

transport properties owing to electron conductivity [47]. The chemical and spectroscopic properties of the molecules are mainly depending on the energy gaps. The frontier molecular orbitals show the electron density for predicting the most reactive position in π-electron systems and also explain several types of reaction in conjugated system [48]. The frontier molecular orbitals (HOMO and LUMO) of free H$_2$ATA are shown in Figure 6. In free H$_2$ATA molecule, the LLCT (Ligand to ligand charge transfer) bands are mainly observed at 185 nm, 224 nm and 365 nm indicating π→π* and n→π* transitions. However, TD-DFT data demonstrated that LLCT bands appeared at 185 - 224 nm. The sharp band appeared at ~224 nm. The molecular orbital contribution (56%) at this band in the gas phase showed the major transitions occurred between the highest occupied molecular orbital (HOMO) to lowest unoccupied molecular orbital+1 (LUMO+1) and the energy gap between HOMO and LUMO+1 was 5.52 eV for H$_2$ATA. An electronic system with a larger HOMO-LUMO gap should be less reactive than one having a smaller gap. The HOMO-LUMO (ΔE_{gap}) gap of the present studied molecule H$_2$ATA is 3.86 eV (Figure 6), indicating the high reactivity. Whereas in the metal complexes, Na$_2$ATA and Na$_4$ATA, the major transitions occur at 267 nm and 199 nm, respectively, due to LLCT (π→π*) transition. The molecular contribution (55%) at 267 nm band for Na$_2$ATA exhibited the major transitions occurred between the highest molecular orbital-3 (HOMO-3) to lowest unoccupied molecular orbital+1 (LUMO+1).

3.6. Global Reactivity Descriptors of H$_2$ATA, Na$_2$ATA and Its Sodium Inserted Complexes (Na$_3$ATA and Na$_4$ATA)

The global reactivity descriptors, e.g. electronegativity (χ), chemical potential (μ), global hardness (η), global softness (s), electrophilicity index (ω) were determined by the conceptual density functional theory on the basis of Koopmans's theorem [49]. The global reactivity descriptors of the titled molecule and its sodium salts were calculated. Global reactivity descriptors were calculated using the energies of frontier molecular orbitals E_{HOMO} and E_{LUMO} as $\chi = -1/2(E_{\text{LUMO}} + E_{\text{HOMO}})$, $\mu = -\chi = 1/2(E_{\text{LUMO}} + E_{\text{HOMO}})$, $\eta = 1/2(E_{\text{LUMO}} - E_{\text{HOMO}})$, s = $1/2\eta$ and $\omega = \mu^2/2\eta$. The energies of frontier molecular orbitals, (E_{LUMO} and E_{HOMO}) and global reactivity descriptors of H$_2$ATA Na$_2$ATA, Na$_3$ATA and Na$_4$ATA are listed in Table 6 and Table 7. The studied molecules, H$_2$ATA and

Figure 6. The frontier molecular orbitals (HOMO and LUMO) of H$_2$ATA.

Table 8. Quantum chemical descriptors of free H$_2$ATA, Na$_2$ATA, Na$_3$ATA and Na$_4$ATA[a].

Complex	χ(eV)	μ(eV)	η(eV)	s(eV)	ω(eV)
H$_2$ATA	4.310	−4.310	1.930	0.259	4.81
Na$_2$ATA	3.130	−3.130	1.662	0.301	2.95
Na$_3$ATA	6.625	−6.625	2.275	0.219	9.65
Na$_4$ATA	9.525	−9.525	2.495	0.200	18.18

[a] χ = electronegativity, μ = chemical potential, η = global hardness, s = global softness, ω = electrophilicity index.

Na$_2$ATA showed a higher HOMO-LUMO gap in gas phase signifying harder molecule. The free H$_2$ATA exhibited higher value for global electrophilicity index, hardnessand electronegativity than Na$_2$ATA (Table 8).

4. Conclusion

In summary, we investigated the structural and vibrational properties of 2-aminoterephthalic acid, disodium 2-aminoterephthalate and inserted sodium complexes using density functional theory (DFT/B3LYP) methods with 6-311++ G(d,p) basis set. The calculated binding energy, enthalpy and Gibbs free energy of Na$_2$ATA revealed that this compound is thermodynamically more stable than other inserted sodium complexes such as Na$_3$ATA or Na$_4$ATA. NBO analysis of disodium 2-aminoterephthalate exhibited the major interaction energy of the O atom with the carbon atoms of the two carboxylate ions as well as its sodium ions. The UV-visible spectrum of the 2-aminoterephthalic acid indicated that molecular orbital contribution (56%) occurred between the highest occupied molecular orbital (HOMO) and the lowest unoccupied molecular orbital+1

(LUMO+1), whereas, in the case of disodium salt, molecular orbital contribution (55%) occurred between the highest molecular orbital-3 (HOMO-3) and lowest unoccupied molecular orbital+1 (LUMO+1). In terms of the global reactivity descriptors, H_2ATA showed higher electronegativity than Na_2ATA. The present computational study of the 2-aminoterephthalic acid and its sodium salts provide strong encouragement for future exploration of functionalized terephthalic acid derivatives as useful material for the safe, low cost, non-toxic, green and easy technology for the production of sodium ion batteries for industrial application.

Acknowledgements

Conflicts of Interest

The authors declare no conflicts of interest regarding the publication of this paper.

References

[1] Qi, W., Shapter, J.G., Wu, Q., Yin, T., Gao, G. and Cui, D. (2017) Nanostructured Anode Materials for Lithium-Ion Batteries: Principal, Recent Progress and Future Perspectives. *Journal of Materials Chemistry A*, **5**, 19521-19540. https://doi.org/10.1039/C7TA05283A

[2] Wang, L.P., Yu, L., Wang, X., Srinivasan, M. and Xu, Z.J. (2015) Recent Developments in Electrode Materials for Sodium-Ion Batteries. *Journal of Materials Chemistry A*, **3**, 9353-9378. https://doi.org/10.1039/C4TA06467D

[3] Hwang, J.-Y., Myung, S.-T. and Sun, Y.-K. (2017) Sodium-Ion Batteries: Present and Future. *Chemical Society Reviews*, **46**, 3529-3614. https://doi.org/10.1039/C6CS00776G

[4] Huang, Y., Zheng, Y., Li, X., Adams, F., Luo, W., Huang, Y. and Hu, L. (2018) Electrode Materials of Sodium-Ion Batteries toward Practical Application. *ACS Energy Letters*, **3**, 1604-1612. https://doi.org/10.1021/acsenergylett.8b00609

[5] Lee, K.T., Ramesh, T.N., Nan, F., Botton, G. and Nazar, L.F. (2011) Topochemical Synthesis of Sodium Metal Phosphate Olivines for Sodium-Ion Batteries. *Chemistry of Materials*, **23**, 3593-3600. https://doi.org/10.1021/cm200450y

[6] Lu, Y., Wang, L., Cheng, J. and Goodenough, J.B. (2012) Prussian Blue: A New Framework of Electrode Materials for Sodium Batteries. *Chemical Communications*, **48**, 6544-6546. https://doi.org/10.1039/c2cc31777j

[7] Jian, Z., Han, W., Lu, X., Yang, H., Hu, Y.-S., Zhou, J., Zhou, Z., Li, J., Chen, W., Chen, D. and Chen, L. (2013) Superior Electrochemical Performance and Storage Mechanism of $Na_3V_2(PO_4)_3$ Cathode for Room-Temperature Sodium-Ion Batteries. *Advanced Energy Materials*, **3**, 156-160. https://doi.org/10.1002/aenm.201200558

[8] Ramasamy, H.V., Kaliyappan, K., Thangavel, R., Aravindan, V., Kang, K., Kim, D.U., Park, Y., Sun, X. and Lee, Y.-S. (2017) Cu-Doped P_2-$Na_{0.5}Ni_{0.33}Mn_{0.67}O_2$ Encapsulated with MgO as a Novel High Voltage Cathode with Enhanced Na-Storage Properties. *Journal of materials Chemistry A*, **5**, 8408-8415.

https://doi.org/10.1039/C6TA10334K

[9] Park, J.-K., Park, G.-G., Kwak, H.H., Hong, S.-T. and Lee, J.-W. (2018) Enhanced Rate Capability and Cycle Performance of Titanium-Substituted P2-Type $Na_{0.67}Fe_{0.5}Mn_{0.5}O_2$ as a Cathode for Sodium-Ion Batteries. *ACS Omega*, **3**, 361-368. https://doi.org/10.1021/acsomega.7b01481

[10] Tang, K., Fu, L., White, R.J., Yu, L., Titirici, M.-M., Antonietti, M. and Maier, J. (2012) Hollow Carbon Nanospheres with Superior Rate Capability for Sodium-Based Batteries. *Advanced Energy Materials*, **2**, 873-877. https://doi.org/10.1002/aenm.201100691

[11] Wang, Y.-X., Chou, S.-L., Liu, H.-K. and Dou, S.-X. (2013) Reduced Graphene Oxide with Superior Cycling Stability and Rate Capability for Sodium Storage. *Carbon*, **57**, 202-208. https://doi.org/10.1016/j.carbon.2013.01.064

[12] Ding, J., Wang, H., Li, Z., Kohandehghan, A., Cui, K., Xu, Z., Zahiri, B., Tan, X., Lotfabad, E.M., Olsen, B.C. and Mitlin, D. (2013) Carbon Nanosheet Frameworks Derived from Peat Moss as High Performance Sodium Ion Battery Anodes. *ACS Nano*, **7**, 11004-11015. https://doi.org/10.1021/nn404640c

[13] Kim, Y., Park, Y., Choi, A., Choi, N.-S., Kim, J., Lee, J., Ryu, J.H., Oh, S.M. and Lee, K.T. (2013) An Amorphous Red Phosphorus/Carbon Composite as a Promising Anode Material for Sodium Ion Batteries. *Advanced Materials*, **25**, 3045-3049. https://doi.org/10.1002/adma.201204877

[14] Zhou, X. and Guo, Y.-G. (2014) Highly Disordered Carbon as a Superior Anode Material for Room-Temaperature Sodium-Ion Batteries. *ChemElectroChem*, **1**, 83-86. https://doi.org/10.1002/celc.201300071

[15] Chen, C., Wen, Y., Hu, X., Ji, X., Yan, M., Mai, L., Hu, P., Shan, B. and Huang, Y. (2015) Na(+) Intercalation Pseudocapacitance in Graphene-Coupled Titanium Oxide Enabling Ultra-Fast Sodium Storage and Long-Term Cycling. *Nature Communications*, **6**, Article No. 6929. https://doi.org/10.1038/ncomms7929

[16] Chen, K.-Y., Zhang, W.-X., Liu, Y., Zhu, H.-P., Duan, J., Xiang, X.-H., Xue, L.-H. and Huang, Y.-H. (2015) Carbon Coated K(0.8)Ti(1.73)Li(0.27)O4: A Novel Anode Material for Sodium-Ion Batteries with a Long Cycle Life. *Chemical Communications*, **51**, 1608-1611. https://doi.org/10.1039/C4CC08051C

[17] Hung, T.-F., Lan, W.-H., Yeh, Y.-W., Chang, W.-S., Yang, C.-C. and Lin, J.-C. (2016) Hydrothermal Synthesis of Sodium Titanium Phosphate Nanoparticles as Efficient Anode Materials for Aqueous Sodium-Ion Batteries. *ACS Sustainable Chemistry & Engineering*, **4**, 7074-7079. https://doi.org/10.1021/acssuschemeng.6b01962

[18] Nyström, G., Razaq, A., Stromme, M., Nyholm, L. and Mihranyan, A. (2009) Ultrafast All-Polymer Paper-Based Batteries. *Nano Letters*, **9**, 3635-3639. https://doi.org/10.1021/nl901852h

[19] Chen, J. and Cheng, F.Y. (2009) Combination of Lightweight Elements and Nanostructured Materials for Batteries. *Accounts of Chemical Research*, **42**, 713-723. https://doi.org/10.1021/ar800229g

[20] Pan, L.J., Yu, G.H., Zhai, D.Y., Lee, H.R., Zhao, W.T., Liu, N., Wang, H.L., Tee, B.C.K., Shi, Y., Cui, Y. and Bao, Z.N. (2012) Hierarchical Nanostructured Conducting Polymer Hydrogel with High Electrochemical Activity. *Proceedings of the National Academy of Sciences of the United States of America*, **109**, 9287-9292. https://doi.org/10.1073/pnas.1202636109

[21] Wu, H., Yu, G., Pan, L., Liu, N., McDowell, M.T., Bao, Z. and Cui, Y. (2013) Stable Li-Ion Battery Anodes by *In-Situ* Polymerization of Conducting Hydrogel to Con-

formally Coat Silicon Nanoparticles. *Nature Communications*, **4**, Article No. 1943. https://doi.org/10.1038/ncomms2941

[22] Wang, S., Wang, L., Zhang, K., Zhu, Z., Tao, Z. and Chen, J. (2013) Organic $Li_4C_8H_2O_6$ Nanosheets for Lithium-Ion Batteries. *Nano Letters*, **13**, 4404–4409. https://doi.org/10.1021/nl402239p

[23] Wang, S., Wang, L., Zhu, Z., Hu, Z., Zhao, Q. and Chen, J. (2014) All Organic Sodium-Ion Batteries with $Na_4C_8H_2O_6$. *Angewandte Chemie International Edition*, **53**, 5892-5896. https://doi.org/10.1002/anie.201400032

[24] Park, Y., Shin, D.-S., Woo, S.H., Choi, N.S., Shin, K.H., Oh, S.M., Lee, K.T. and Hong, S.Y. (2012) Sodium Terephthalate as an Organic Anode Material for Sodium Ion Batteries. *Advanced Materials*, **24**, 3562-3567. https://doi.org/10.1002/adma.201201205

[25] Han, M.H., Gonzalo, E., Singh, G. and Rojo, T. (2015) A Comprehensive Review of Sodium Layered Oxides: Powerful Cathodes for Na-Ion Batteries. *Energy & Environmental Science*, **8**, 81-102. https://doi.org/10.1039/C4EE03192J

[26] Mayo, M., Griffith, K.J., Pickard, C.J. and Morris, A.J. (2016) *Ab Initio* Study of Phosphorus Anodes for Lithium- and Sodium-Ion Batteries. *Chemistry of Materials*, **28**, 2011-2021. https://doi.org/10.1021/acs.chemmater.5b04208

[27] Stratford, J.M., Mayo, M., Allan, P.K., Pecher, O., Borkiewicz, O.J., Wiaderek, K.M., Chapman, K.W., Pickard, C.J., Morris, A.J. and Grey, C.P. (2017) Investigating Sodium Storage Mechanisms in Tin Anodes: A Combined Pair Distribution Function Analysis, Density Functional Theory, and Solid-State NMR Approach. *Journal of the American Chemical Society*, **139**, 7273-7286. https://doi.org/10.1021/jacs.7b01398

[28] Li, J., Yan, D., Lu, T., Qin, W., Yao, Y. and Pan, L. (2017) Significantly Improved Sodium-Ion Storage Performance of CuS Nanosheets Anchored into Reduced Graphene Oxide with Ether-Based Electrolyte. *ACS Applied Materials & Interfaces*, **9**, 2309-2316. https://doi.org/10.1021/acsami.6b12529

[29] Eddaoudi, M., Kim, J., Rosi, N., Vodak, D., Wachter, J., O'Keeffe, M. and Yaghi, O.M. (2002) Systematic Design of Pore Size and Functionality in Isoreticular MOFs and Their Application in Methane Storage. *Science*, **295**, 469-472. https://doi.org/10.1126/science.1067208

[30] Rowsell, J.L.C. and Yaghi, O.M. (2006) Effects of Functionalization, Catenation, and Variation of the Metal Oxide and Organic Linking Units on the Low-Pressure Hydrogen Adsorption Properties of Metal-Organic Frameworks. *Journal of the American Chemical Society*, **128**, 1304-1315. https://doi.org/10.1021/ja056639q

[31] Bhattacharjee, S., Yang, D.-A. and Ahn, W.-S. (2011) A New Heterogeneous Catalyst for Epoxidation of Alkenesvia One-Step Post-Functionalization of IRMOF-3 with a Manganese (II) Acetylacetonate Complex. *Chemical Communications*, **47**, 3637-3639. https://doi.org/10.1039/c1cc00069a

[32] Kim, J., McNamara, N.D., Her, T.H. and Hicks, J.C. (2013) Carbothermal Reduction of Ti-Modified IRMOF-3: An Adaptable Synthetic Method to Support Catalytic Nanoparticles on Carbon. *ACS Applied Materials & Interfaces*, **5**, 11479-11487. https://doi.org/10.1021/am404089v

[33] Rostamnia, S. and Xin, H. (2014) Basic Isoreticular Metal-Organic Framework (IRMOF-3) Porous Nanomaterial as a Suitable and Green Catalyst for Selective Unsymmetrical Hantzsch Coupling Reaction. *Applied Organometallic Chemistry*, **28**, 359-363. https://doi.org/10.1002/aoc.3136

[34] Lee, Y.-R., Cho, S.-M., Ahn, W.-S., Lee, C.-H., Lee K.-H. and Cho, W.-S. (2015) Fa-

cile Synthesis of an IRMOF-3 Membrane on Porous Al_2O_3 Substrate via a Sono-chemical Route. *Microporous and Mesoporous Materials*, **213**, 161-168. https://doi.org/10.1016/j.micromeso.2015.04.021

[35] Bhattacharjee, S. (2018) Synthesis and Application of Layered Double Hydroxide-Hosted 2-Aminoterephthalate for the Knoevenagel Condensation Reaction. *Inorganic and Nano-Metal Chemistry*, **48**, 340-346. https://doi.org/10.1080/24701556.2019.1567538

[36] Britt, D., Tranchemontagne, D. and Yaghi, O.M. (2008) Metal-Organic Frameworks with High Capacity and Selectivity for Harmful Gases. *Proceedings of the National Academy of Sciences of the United States of America*, **105**, 11623-11627. https://doi.org/10.1073/pnas.0804900105

[37] Karabacak, M., Cinar, M., Unal, Z. and Kurt, M. (2010) FT-IR, UV Spectroscopic and DFT Quantum Chemical Study on the Molecular Conformation, Vibrational and Electronic Transitions of 2-Aminoterephthalic Acid. *Journal of Molecular Structure*, **982**, 22-27. https://doi.org/10.1016/j.molstruc.2010.07.033

[38] Renault, St., Oltean, V.A., Ebadi, M., Edström, K. and Brandell, D. (2017) Dilithium 2-Aminoterephthalate as a Negative Electrode Material for Lithium-Ion Batteries. *Solid State Ionics*, **307**, 1-5. https://doi.org/10.1016/j.ssi.2017.05.005

[39] Becke, A.D. (1993) Density-Functional Thermochemistry. III. The Role of Exact Exchange. *Journal of Chemical Physics*, **98**, 5648-5652. https://doi.org/10.1063/1.464913

[40] Matin, M.A., Chitumalla, R.K., Lim, M., Gao, X. and Jang, J.K. (2015) Density Functional Theory Study on the Cross-Linking of Mussel Adhesive Proteins. *Journal of Physical Chemistry B*, **119**, 5496-5504. https://doi.org/10.1021/acs.jpcb.5b01152

[41] Frisch, M.J., Trucks, G.W., Schlegel, H.B., Scuseria, G.E., Robb, M.A., Cheeseman, J.R., Scalmani, G., Barone, V., Petersson, G.A., Nakatsuji, H., Li, X., Caricato, M., Marenich, A.V., Bloino, J., Janesko, B.G., Gomperts, R., Mennucci, B., Hratchian, H.P., Ortiz, J.V., Izmaylov, A.F., Sonnenberg, J.L., Williams-Young, D., Ding, F., Lipparini, F., Egidi, F., Goings, J., Peng, B., Petrone, A., Henderson, T., Ranasinghe, D., Zakrzewski, V.G., Gao, J., Rega, N., Zheng, G., Liang, W., Hada, M., Ehara, M., Toyota, K., Fukuda, R., Hasegawa, J., Ishida, M., Nakajima, T., Honda, Y., Kitao, O., Nakai, H., Vreven, T., Throssell, K., Montgomery, J.A., Peralta, J.E., Ogliaro, F., Bearpark, M.J., Heyd, J.J., Brothers, E.N., Kudin, K.N., Staroverov, V.N., Keith, T.A., Kobayashi, R., Normand, J., Raghavachari, K., Rendell, A.P., Burant, J.C., Iyengar, S.S., Tomasi, J., Cossi, M., Millam, J.M., Klene, M., Adamo, C., Cammi, R., Ochterski, J.W., Martin, R.L., Morokuma, K., Farkas, O., Foresman, J.B. and Fox, D.J. (2016) Gaussian 16, Revision B.01. Gaussian, Inc., Wallingford.

[42] Lakraychi, A.E., Dolhem, F., Djedaïni-Pilard, F., Thiam, A., Frayret, C. and Becuwe, M. (2017) Decreasing Redox Voltage of Terephthalate-Based Electrode Material for Li-Ion Battery Using Substituent Effect. *Journal Power Sources*, **359**, 198-204. https://doi.org/10.1016/j.jpowsour.2017.05.046

[43] He, J., Zhang, Y., Yu, J., Pan, Q. and Xu, R. (2006) Two 2-D 36 Tessellated Metal-Organic Frameworks Constructed from Trimetallic Clusters and Dicarboxylate-Ditopic Links. *Materials Research Bulletin*, **41**, 925-933. https://doi.org/10.1016/j.materresbull.2006.01.018

[44] Garibay, S.J., Wang, Z. and Cohen, S.M. (2010) Evaluation of Heterogeneous Metal-Organic Framework Organocatalysts Prepared by Postsynthetic Modification. *Inorganic Chemistry*, **49**, 8086-8091. https://doi.org/10.1021/ic1011549

[45] Liu, L.L., *et al.* (2012) Engineering Metal-Organic Frameworks Immobilize Gold

Catalysts for Highly Efficient One-Pot Synthesis of Propargylamines. *Green Chemistry*, **14**, 1710-1720. https://doi.org/10.1039/c2gc35284b

[46] Thompson, H.W. and Torkington, P. (1945) The Vibrational Spectra of Esters and Ketones. *Journal of the Chemical Society*, **171**, 640-645. https://doi.org/10.1039/jr9450000640

[47] Fukui, K. (1982) Role of Frontier Orbitals in Chemical Reactions. *Science*, **218**, 747-754. https://doi.org/10.1126/science.218.4574.747

[48] Fukui, K., Yonezawa, T. and Shingu, H. (1952) A Molecular Orbital Theory of Reactivity in Aromatic Hydrocarbons. *The Journal of Chemical Physics*, **20**, 722-725. https://doi.org/10.1063/1.1700523

[49] Koopmans, T. (1934) Über Die Zuordnung Von Wellenfunktionen Und EigenwertenZu Den EinzelnenElektronenEines Atoms. *Physica*, **1**, 104-113. https://doi.org/10.1016/S0031-8914(34)90011-2